Article

How to Make a Better Magnet? Insertion of Additional Bridging Ligands into a Magnetic Coordination Polymer

Gabriela Handzlik[ID] **and Dawid Pinkowicz** *[ID]

Faculty of Chemistry, Jagiellonian University, Gronostajowa 2, 30-387 Kraków, Poland;
gabriela.handzlik@uj.edu.pl
* Correspondence: dawid.pinkowicz@uj.edu.pl; Tel.: +48-16-686-2457

check for
updates

Abstract: A three-dimensional cyanide-bridged coordination polymer based on Fe^{II} ($S = 2$) and Nb^{IV} ($S = 1/2$) $\{[Fe^{II}(H_2O)_2]_2[Nb^{IV}(CN)_8]\cdot4H_2O\}_n$ (**Fe₂Nb**) was modified at the self-assembly stage by inserting an additional formate $HCOO^-$ bridge into its cyanide framework. The resulting mixed-bridged $\{(NH_4)[(H_2O)Fe^{II}\text{-}(\mu\text{-}HCOO)\text{-}Fe^{II}(H_2O)][Nb^{IV}(CN)_8]\cdot3H_2O\}_n$ (**Fe₂NbHCOO**) exhibited additional Fe^{II}-HCOO-Fe^{II} structural motifs connecting each of the two Fe^{II} centers. The insertion of $HCOO^-$ was possible due to the substitution of some of the *aqua* ligands and crystallization water molecules in the parent framework by formate anions and ammonium cations. The formate molecular bridge not only shortened the distance between Fe^{II} ions in **Fe₂NbHCOO** from 6.609 Å to 6.141 Å, but also created additional magnetic interaction pathways between the magnetic centers, resulting in an increase in the long range magnetic ordering temperature from 43 K for **Fe₂Nb** to 58 K. The mixed-bridged **Fe₂NbHCOO** also showed a much broader magnetic hysteresis loop of 0.102 T, compared to 0.013 T for **Fe₂Nb**.

Keywords: ferrimagnetism; long-range magnetic ordering; iron(II); octacyanidoniobate(IV); coordination polymers

1. Introduction

The rational design of crystalline molecular magnets enables the combination of magnetism (ferromagnetism) with other properties within a single material. The additional functionalities co-exist or are strongly coupled with the magnetic ordering, providing a convenient route to multifunctionality [1]. In terms of future technological applications, it is crucial to develop new strategies towards higher magnetic ordering temperatures in molecular magnets [2] to eliminate the need for expensive cooling resources like liquid helium. Efforts thus far have focused mainly on Prussian blue analogs [3] and cyanido-bridged materials based on hepta- or octacyanidometallates of 4*d* and 5*d* metal ions [4,5]. This is due to the ability of CN^- to efficiently mediate moderate-to-strong magnetic interactions between the bridged paramagnetic metal ions. Most of the room-temperature molecular magnets are based on V^{II}/V^{III} and Cr^{III} metal ions, where the magnetic coupling was found to be the strongest [6–12]. Unfortunately, these compounds are often obtained as amorphous powders and are air-sensitive, therefore, there is still a high demand for air-stable, crystalline, high-T_c, molecule-based magnets. One way to achieve this is changing the metal centers (spins and coupling constants). Here, a slightly different approach is proposed based on increasing the number of the closest magnetic neighbors. This approach is dictated by the molecular field theory Equation (1) [13], where the T_c depends on three factors: the coupling constant J_{AB} between the two metal centers A and

B, the spin values S_A and S_B and the number of the closest magnetic neighbors n_A and n_B (k_B is the Boltzmann constant).

$$T_c = \frac{2\sqrt{n_A n_B}\left|J_{AB}\right|\sqrt{S_A(S_A+1)S_B(S_B+1)}}{3k_B}, \tag{1}$$

The aim of our research was to modify the well-known compound $\{[Fe^{II}(H_2O)_2]_2[Nb^{IV}(CN)_8]\cdot4H_2O\}_n$ (**Fe₂Nb**) [14] by inserting additional bridging ligands connecting the Fe^{II} ions in order to increase the number of the nearest magnetic neighbors, and re-inforce the existing long-range magnetic ordering. The implemented changes were similar to the modification of the Mn^{II}-Nb^{IV} analogue $\{[Mn^{II}(H_2O)_2]_2[Nb^{IV}(CN)_8]\cdot4H_2O\}_n$, described previously [15]. The insertion of formate into the newly obtained mixed-bridged compound $\{(NH_4)[(H_2O)Fe^{II}\text{-}(\mu\text{-}HCOO)\text{-}Fe^{II}(H_2O)][Nb^{IV}(CN)_8]\cdot3H_2O\}_n$ (**Fe₂NbHCOO**) led to a very significant increase of the critical temperature T_c from 43 K (**Fe₂Nb** parent framework) to 58 K, and a larger coercive field.

2. Results and Discussion

2.1. Synthesis and X-ray Crystal Structure Description

The insertion of additional formate anions into the three-dimensional (3D), CN-bridged parent framework of **Fe₂Nb** at the self-assembly stage resulted in the formation of **Fe₂NbHCOO** with mixed 3*d*-4*d* and 3*d*-3*d* metal bridging. The key to its formation was a large excess of ammonium formate in the solution of the building blocks: Mohr's salt and potassium octacyanidoniobate(IV) dihydrate. The formation of the desired product was fully confirmed by single crystal X-ray diffraction structural analysis (sc-XRD; Figure 1 and Table 1), infrared spectroscopy (IR), elemental analysis (EA), and powder X-ray diffraction (PXRD).
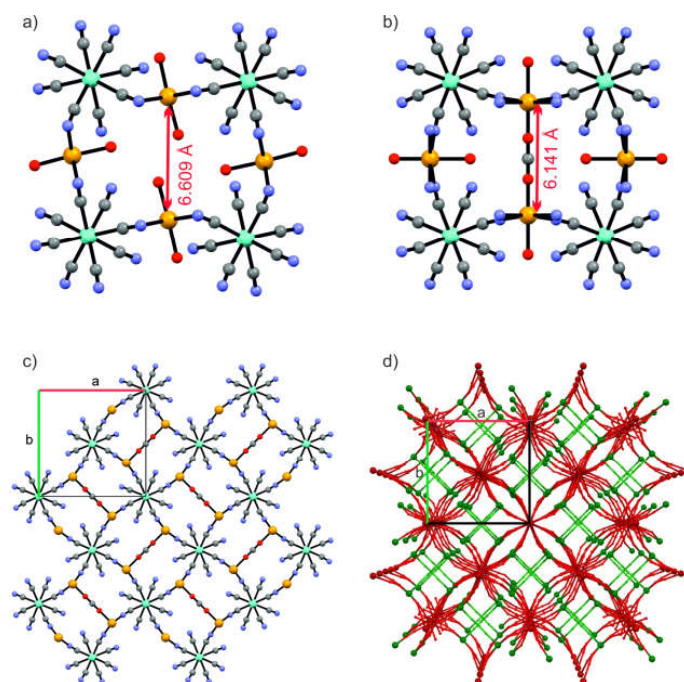

Figure 1. Structural diagrams showing the potential "cavity" between adjacent Fe^{II} ions in the parent framework **Fe₂Nb** (**a**), the additional formate bridge occupying the "cavity" in **Fe₂NbHCOO** (**b**), a slice of **Fe₂NbHCOO** crystal packing parallel to the *ab* crystallographic plane (**c**), and a packing diagram presenting the three-dimensional (3D) CN-bridged coordination framework (red) cross-linked by local formate bridges (green) (**d**). Note: Nb—cyan, Fe—yellow, C—gray, N—blue, and $O_{formate}$—red. Hydrogen and oxygen atoms of water molecules have been omitted for the sake of clarity.

Table 1. Sc-XRD structural, solution and refinement parameters for **Fe$_2$NbHCOO**.

Formula	C$_9$HFe$_2$N$_9$NbO$_7$
Temperature, K	296(2)
λ, Å	0.71073 Å
Molecular weight, g/mol	551.80
Crystallographic system	tetragonal
Space group	*I4cm*
Unit cell	a = 11.8782(12) Å b = 13.2770(14) Å
Volume V, Å^3	1873.3(4)
Z	4
Density ρ_{calc}, g/cm^3	1.957
F (000)	1068
θ, deg	3.4–28.0
Abs. coeff. μ, mm^{-1}	2.18
Data/parameters /restrains	1211/81/8
R [$F^2 > 2\sigma(F^2)$]	0.032
wR (F^2)	0.064
GOF on F^2	1.103
Flack parameter	0.472(25)
max/min resid. density, e· Å^{-3}	1.13/−0.59
Reflections collected	13274
Unique reflections	1211
R_{int}	0.048
Completeness, %	99.6

Fe$_2$NbHCOO is isostructural with its Mn^{II} analogue {(NH$_4$)[(H$_2$O)Mn^{II}-(μ-HCOO)-Mn^{II}(H$_2$O)][Nb^{IV}(CN)$_8$]·3H$_2$O}$_n$ (**Mn$_2$NbHCOO**) [15]. The coordination framework of **Fe$_2$NbHCOO** becomes anionic compared to **Fe$_2$Nb,** due to the insertion of negatively charged formate. As such, its electroneutrality is maintained by a simultaneous incorporation of an ammonium cation, which replaces one of the crystallization water molecules present in the parent compound.

Insertion of formate anions causes mild changes in the geometry of the CN-framework of **Fe$_2$NbHCOO**, compared to the parent **Fe$_2$Nb**. However, a noticeable change occurred between the adjacent Fe^{II} centers, where the formate ion was bound (Figure 1b), the Fe^{II}···Fe^{II} distance was shortened by 0.468 Å (from 6.609 Å to 6.141 Å). The corresponding change in the **Mn$_2$NbHCOO [15]** compared to its Mn^{II}-Nb^{IV} parent [16] was smaller, shortening by only 0.337 Å (from 6.590 Å to 6.253 Å). A comparison of the most important distances and angles in **Fe$_2$NbHCOO** and **Fe$_2$Nb** is presented in Table 2. The cyanide bridges in **Fe$_2$NbHCOO** were slightly less bent compared to **Fe$_2$Nb**, while other structural parameters were quite similar (except for the aforementioned Fe···Fe distances).

Table 2. Comparison of selected distances (Å) and angles (°) in the parent framework and modified **Fe₂NbHCOO**.

Atom Names	Fe₂Nb	Fe₂NbHCOO
Nb···Fe	5.409 5.508	5.461 5.480
Nb···Fe$_{av}$	5.459	5.471
Fe···Fe	6.609(1)	6.141(1)
Fe-N$_{CN}$	2.144(2) 2.175(2)	2.119(10) 2.171(10)
Fe-N-C	154.5(2) 167.5(2)	157.8(11) 170.0(9)
Nb-C-N	174.6(2) 176.7(2)	173.0(10) 178.4(11)
Fe-O$_{aq}$	2.099(3) 2.130(3)	2.191(9)
Fe-O$_{HCOO}$	-	1.977(9)

In both **Fe₂NbHCOO** and **Fe₂Nb,** each $[Nb^{IV}(CN)_8]^{4-}$ was connected to eight nearly octahedral $[Fe^{II}(CN)_4(H_2O)L]$ moieties (L = H_2O for **Fe₂Nb** and L = formate for **Fe₂NbHCOO**). The coordination geometry of Nb^{IV} in **Fe₂NbHCOO** was slightly closer to an ideal square antiprism than in **Fe₂Nb,** according to the continuous shape measure analysis executed using SHAPE software [17]. Conversely, the geometry of the octahedral Fe^{II} centers was much more distorted in **Fe₂NbHCOO** due to the strain imposed by the bridging formate anion (Figure 1a,b and Table 3), which might lead to a completely different magnetic anisotropy.

Table 3. Analysis of the coordination spheres of Fe^{II} and Nb^{IV} ions in **Fe₂Nb** and **Fe₂NbHCOO**.

Nb^{IV}	Square antiprism (SAPR-8)	0.192	0.113
Fe^{II}	Octahedron (OC-6)	0.161	0.562

The insertion of the additional formate bridge into the parent **Fe₂Nb** framework changed the symmetry from a centrosymmetric *I4/m* to a non-centrosymmetric *I4cm*. The structure of **Fe₂NbHCOO** was refined as an inversion twin with the following scales: 0.49(10) and 0.51(10). The asymmetric unit (Figure 2) was comprised of Nb^{IV} and Fe^{II} ions linked with a CN^- ligand (C2N2). The second CN^- ligand (C1N1) in the asymmetric unit connected the Fe^{II} ion with the next Nb^{IV} ion in the structure. The asymmetric unit also included an *aqua* ligand coordinated to Fe^{II} (O1) and half of the bridging formate anion (C3O2). There were also two oxygen atoms of the crystallization water molecules (O3 with occupancy 0.5 and O4 with occupancy 1.0), and a nitrogen atom of the ammonium cation (N3 with 0.5 occupancy in the same position as O3). H-atoms could not be located from the Fourier difference map. The presence of the ammonium cation was confirmed by IR spectroscopy (see below) and is consistent with the elemental analysis (EA) results.
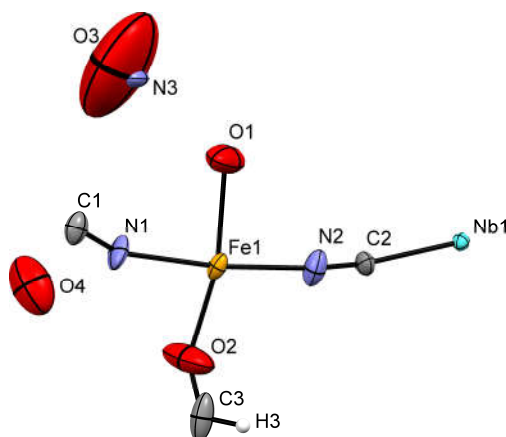
Figure 2. Asymmetric unit of **Fe₂NbHCOO**.

2.2. IR Spectroscopy

The infrared (IR) spectrum of **Fe₂NbHCOO** (Figure 3) exhibited bands typical for the parent framework: two bands characteristic for stretching (3576 cm^{-1}) and bending (1635 cm^{-1}) vibrations of O-H, and a strong band characteristic for stretching vibrations of CN$^-$ ligands (2141 cm^{-1}). Additional specific bands as compared to the parent framework indicate the presence of the inserted formate anions (1584 cm^{-1}, 1383 cm^{-1}, 1365 cm^{-1} and 812 cm^{-1}) and the ammonium cations (3261 cm^{-1} and 1403 cm^{-1}).
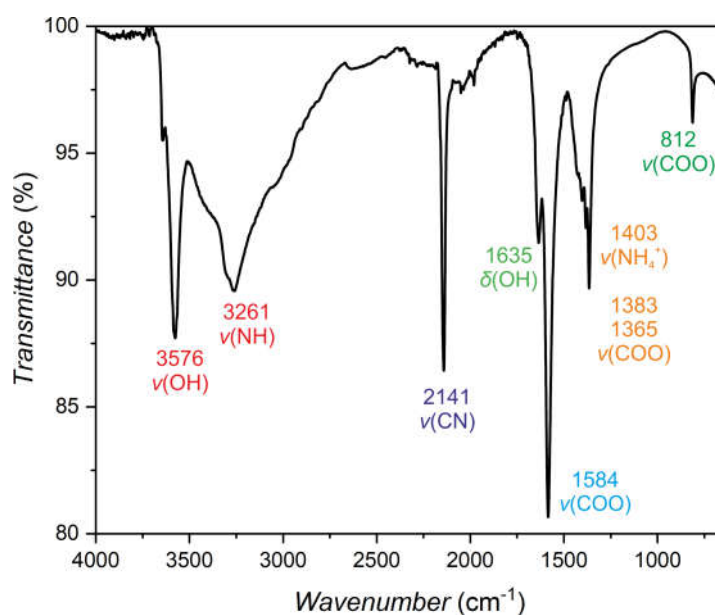
Figure 3. IR spectrum of **Fe₂NbHCOO**.

2.3. Identity and Purity Confirmation by Powder X-ray Diffraction

The identity and purity of the bulk sample of **Fe₂NbHCOO** was confirmed by powder X-ray diffraction measurements (Figure 4). The experimental PXRD diffraction patterns were in very good agreement with the simulated results from the sc-XRD structural model obtained at room temperature.
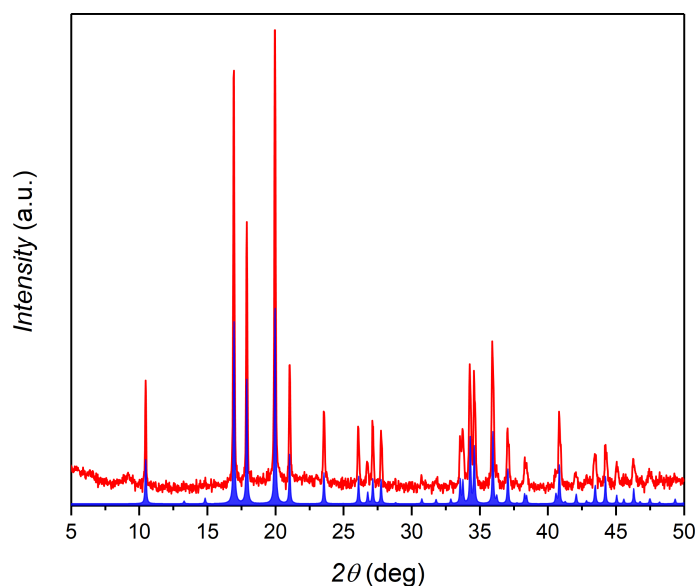
Figure 4. Experimental (red) and simulated from the single-crystal structural model (blue) powder X-ray diffraction patterns for **Fe₂NbHCOO** (the broad peak at 8° is from the glass capillary—the sample holder).

2.4. Magnetic Properties

The shape of the $\chi T(T)$ dependence for **Fe₂NbHCOO** recorded in the 2–300 K range at 0.1 T magnetic field (Figure 5) suggests the presence of a long-range magnetic ordering in this system below 70 K (discussed below). The experimental χT value at 300 K of 8.31 cm³·K·mol⁻¹ was slightly lower than the expected 9.02 cm³·K·mol⁻¹ for two Fe^{II} ($S = 2$), assuming $g_{Fe} = 2.4$, and one Nb^{IV} ($S = \frac{1}{2}$), assuming $g_{Nb} = 2.0$. This was most probably caused by the presence of antiferromagnetic interactions within the Nb^{IV}-CN-Fe^{II} coordination framework. χT increased significantly as the temperature was lowered to reach a maximum value of 889 cm³·K·mol⁻¹ at 45 K, confirming the long-range magnetic ordering.

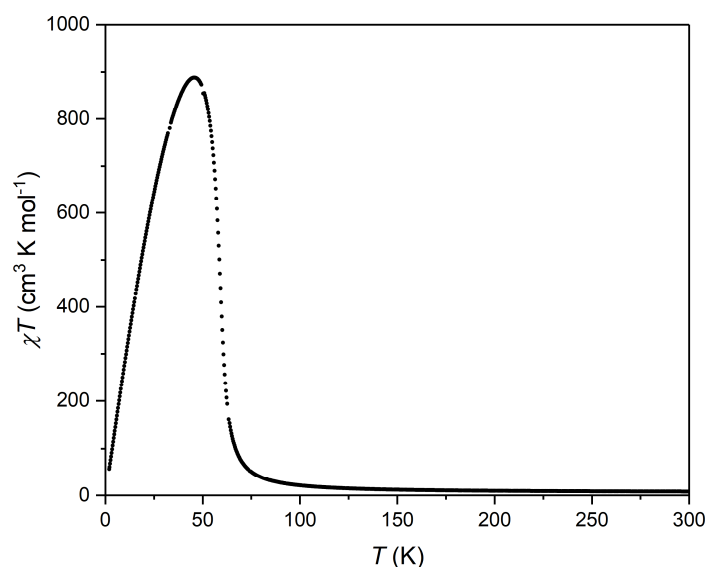**Figure 5.** Temperature dependence of the molar magnetic susceptibility and temperature product for **Fe₂NbHCOO** at $H = 0.1$ T.

The magnetization vs. temperature $M(T)$ curves recorded in the zfc-fc (zero field-cooled, field-cooled) modes at 0.3 mT for **Fe₂NbHCOO** are presented in Figure 6. The most striking

feature is the significant increase of the magnetization at 58 K, which constitutes the long-range magnetic ordering temperature T_c for this system. The critical temperature T_c was defined as the zfc-fc bifurcation point and was confirmed by the position of the maximum of the AC (alternating current) magnetic susceptibility signal χ' at 57.5 K (Figure 7). There was essentially no frequency dependence of the in-phase and out-of-phase AC susceptibilities at the magnetic ordering temperature, which supports the claim that the reported compound is a magnetically ordered system. However, a slight frequency drift below 50 K indicates some dynamic processes taking place in the compound. Understanding this behavior will require further measurements using more advanced techniques (i.e., muon spin spectroscopy).
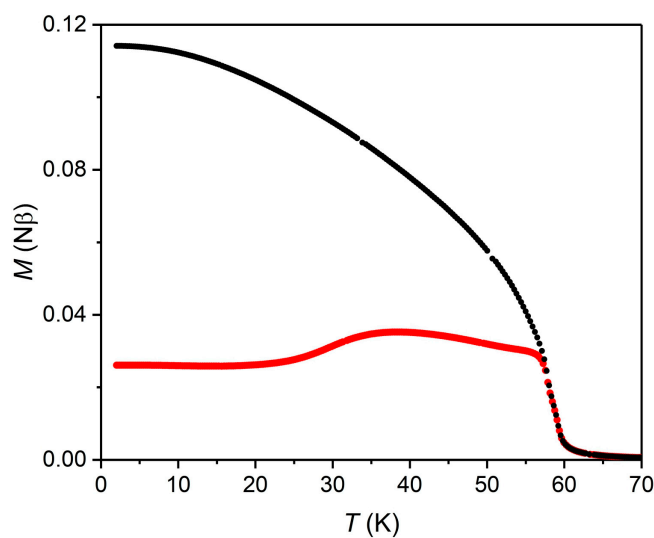

Figure 6. Temperature dependence of the molar magnetization measured in the zfc-fc (**red** and **black** points, respectively) modes for **Fe₂NbHCOO**.
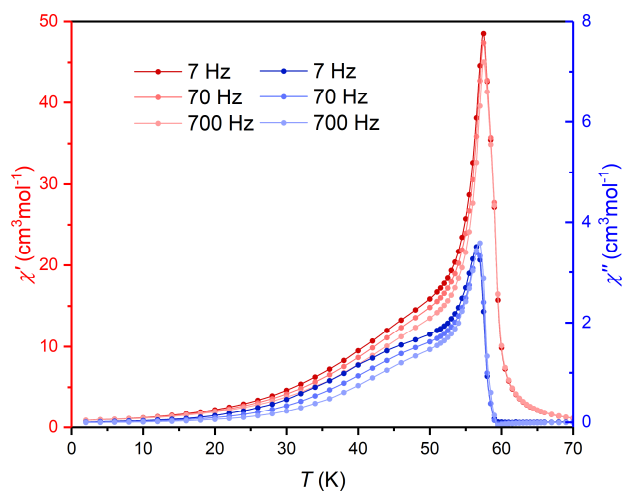

Figure 7. Temperature dependence of the in-phase and out-of-phase AC magnetic susceptibility of **Fe₂NbHCOO** at $H_{AC} = 0.1$ mT and at three different frequencies (7, 70 and 700 Hz).

The magnetic field dependence of the molar magnetization for **Fe₂NbHCOO** (recorded up to 7 T at $T = 2.0$ K) is presented in Figure 8. The magnetization curve showed a fast increase to circa 4.5 Nβ at 0.2 T, followed by a further slower increase and a saturation value of ca. 8.8 Nβ at 7.0 T. This was similar to the value obtained for the parent **Fe₂Nb** [14], and close to the expected 8.6 Nβ for two high-spin Fe^{II} ($S = 2$, $g_{Fe} = 2.4$) antiferromagnetically coupled with Nb^{IV} ion ($S = \frac{1}{2}$, $g_{Nb} = 2.0$). This suggests that **Fe₂NbHCOO** exhibits long-range ferrimagnetic ordering. **Fe₂NbHCOO** exhibited a magnetic hysteresis

loop (Figure 8, inset) with the coercive field H_c = 102 mT and the remanence M_R = 4.8 Nβ. Both values were much larger than the parent framework **Fe₂Nb** (H_c = 13 mT and M_R = 1.24 Nβ). The significant increase of the magnetic ordering temperature and a larger coercive field/remanence of **Fe₂NbHCOO** compared to the parent **Fe₂Nb** were most likely caused by the inserted bridging formate connecting the neighboring Fe^{II} ions. This formate bridge must promote the Fe^{II} ions magnetic anisotropy change and most probably additional local ferromagnetic interactions between them, which work in concert with the postulated ferrimagnetic structure of the CN-bridged framework (Figure 9). Nevertheless, an unlikely scenario where strong ferromagnetic ordering within the Nb^{IV}-CN-Fe^{II} framework [14] is accompanied by very weak antiferromagnetic interactions through Fe^{II}-HCOO-Fe^{II} pairs is also possible. Please note that the Mn^{II}-based analog $\{(NH_4)[(H_2O)Mn^{II}$-(μ-OOCH)-$Mn^{II}(H_2O)][Nb^{IV}(CN)_8]\cdot 3H_2O\}_n$ (**Mn₂NbHCOO**) that we recently reported [15] showed a significant lowering of the T_c from 49 K to 45 K compared to its $\{[Mn^{II}(H_2O)_2]_2[Nb^{IV}(CN)_8]\cdot 4H_2O\}_n$ (**Mn₂Nb**) parent framework, due to the antiferromagnetic interactions transmitted through the Mn^{II}-HCOO-Mn^{II} motifs.
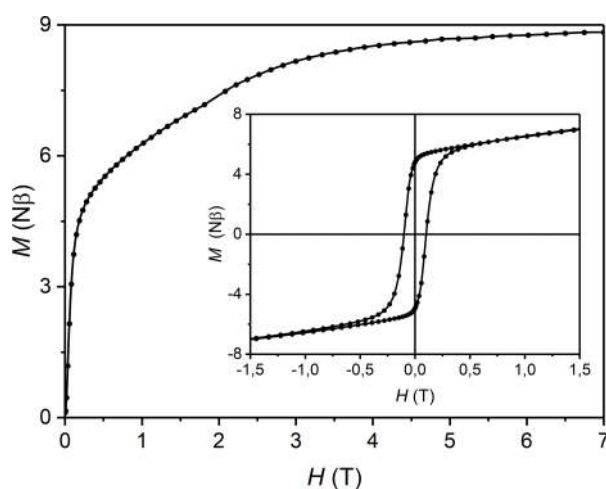

Figure 8. The magnetic field dependence of the molar magnetization of **Fe₂NbHCOO** recorded at 2.0 K in the 0–7 T range and the magnetic hysteresis loop at the same temperature (inset).
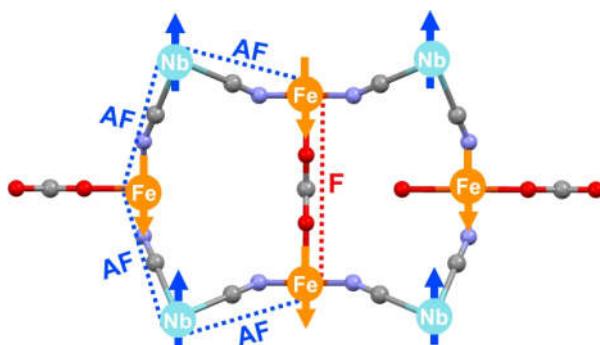

Figure 9. Schematic representation of the postulated ferrimagnetic structure of **Fe₂NbHCOO** with an antiparallel alignment of the Nb^{IV} and Fe^{II} magnetic moments. The ferromagnetic interactions transmitted through the newly introduced Fe^{II}-HCOO-Fe^{II} structural motifs work in concert with the antiferromagnetic coupling within the -Nb^{IV}-CN-Fe^{II}- 3D skeleton.

3. Materials and Methods

3.1. Materials

Chemicals of analytical grade were purchased from commercial sources (Sigma-Aldrich Co., St. Louis, MO, USA) and used as received. $K_4[Nb(CN)_8]\cdot 2H_2O$ was synthesized according to the last reported procedure [18]. All operations were carried out in an ambient atmosphere.

3.2. Synthesis of {(NH_4)[(H_2O)Fe^{II}-(μ-HCOO)-Fe^{II}(H_2O)][Nb^{IV}(CN)_8]·3H_2O}_n (**Fe_2NbHCOO**)

A water (160 mL) solution of $HCOONH_4$ (1.26 g, 20.0 mmol) with a small amount of ascorbic acid (ca. 10–15 mg) was prepared. Half of the volume of this solution was used to dissolve $K_4[Nb(CN)_8]·2H_2O$ (149.1 mg, 0.30 mmol), and the other half was used to dissolve $(NH_4)_2Fe(SO_4)_2·6H_2O$ (235.3 mg, 0.60 mmol). After adding the greenish solution of Mohr's salt to the yellow solution of potassium octacyanidoniobiate(IV), the resulting orange mixture was left for one day for crystallization. Dark purple crystals (60.2 mg, 35%) of **Fe_2NbOOCH** were isolated by repeated decantation with distilled water followed by ethanol (92%), and were dried for a short while in air (the compound is slightly sensitive to oxygen and needs to be stored at low temperature). We found C, 18.81; H, 2.59; N, 21.40. $C_9H_{15}Fe_2N_9NbO7$ (565.87 g/mol) requires C, 19.10; H, 2.67; N, 22.28%. Slightly lower N content is caused by the air-sensitivity of the compound. IR (ν_{max}/cm^{-1}): 3576 s ν(OH), 3261 s ν(NH), 2141 s ν(CN), 1635 m δ(OH), 1584 vs ν(COO), 1403 ν(NH_4^+), 1383 m and 1365 ν(COO), and 812 ν(COO).

3.3. Single-Crystal X-ray Diffraction

The single crystal diffraction data for **Fe_2NbHCOO** was collected on a Bruker D8 Quest Eco Photon50 CMOS machine equipped with a Mo Kα radiation source and a graphite monochromator (λ = 0.71073 Å). Measurements were performed at ambient temperature (details in Table 1). Data reduction and unit cell determination were carried out using SAINT and SADABS (Apex3 package). Absorption correction using the multi-scan method was applied for all reflection intensities. The structure was solved using direct methods (Apex3 package). Non-hydrogen atoms were refined anisotropically using weighted full-matrix least-squares on F^2 [19,20]. The crystallographic data is summarized in Table 1. CCDC 1859396 (**Fe_2NbHCOO**) contains the supplementary crystallographic data for this paper. This data can be obtained free of charge from the Cambridge Crystallographic Data Centre via ww.ccdc.cam.ac.uk/data_request/cif.

3.4. Magnetic Measurements

Magnetic measurements were performed using a Quantum Design MPMS-3 Evercool magnetometer equipped with a 7 T superconducting magnet. The sample was loaded into a double polypropylene bag and sealed. The magnetic susceptibility was corrected for the diamagnetic contribution of the sample holder and the diamagnetism of the samples themselves using Pascal constants.

3.5. Other Physical Measurements and Calculations

Infrared spectra were collected on Nicolet iS 5 FT-IR spectrometer (Thermo Fisher Scientific, Wltham, MA, USA) in the range 4000–650 cm^{-1}. Powder X-ray diffraction experiments (PXRD) were carried out using PANalytical X'Pert Pro MPD diffractometer (Cu Kα radiation, Malvern PANalytical, Royston, UK) at ambient temperature for dry well-ground samples loaded into a narrow diameter borosilicate-glass capillary (0.7 mm). Elemental analysis was performed using an ELEMENTAR Vario Micro Cube CHNS analyzer (Elementar, Langenselbold, Germany). Continuous shape measure analysis for coordination spheres of Nb^{IV} and Fe^{II} was performed using the SHAPE software [21]. The results are summarized in Table 3.

4. Conclusions

A modification of the structure and magnetic properties of a parent coordination polymer **Fe_2Nb** was performed at the self-assembly stage by "forcing" an additional bridging formate anion into its structure. The formate anion formed direct coordination connections with two adjacent Fe^{II} centers within the CN-bridged Fe^{II}-Nb^{IV} framework. The presence of this additional molecular bridge promoting ferromagnetic interactions between iron(II) centers reinforced the ferrimagnetic

structure of the Fe^{II}-Nb^{IV} framework, and made **Fe₂NbHCOO** a much better magnet than the parent **Fe₂Nb**. Our approach demonstrates a new efficient route towards molecular magnets with higher critical temperatures.

Author Contributions: D.P. conceived and designed the experiments and performed the magnetic measurements; G.H. synthesized the compounds and performed the single crystal XRD structural analysis; and D.P. and G.H. analyzed the data and wrote the paper together.

Conflicts of Interest: The authors declare no conflict of interest.

References

1. Pinkowicz, D.; Czarnecki, B.; Reczyński, M.; Arczyński, M. Multifunctionality in Molecular Magnetism. *Sci. Prog.* **2015**, *98*, 346–378. [CrossRef] [PubMed]

2. Miller, J.S.; Ohkoshi, S. High-T_c Ordered Molecular Magnets. In *Molecular Magentic Materials. Concepts and Applications*, 1st ed.; Sieklucka, B., Pinkowicz, D., Eds.; Wiley: Weinheim, Germany, 2017; pp. 161–186, ISBN 978-3-527-33953-2.

3. Tokoro, H.; Ohkoshi, S. Novel magnetic functionalities of Prussian blue analogs. *Dalton Trans.* **2011**, *40*, 6825–6833. [CrossRef] [PubMed]

4. Nowicka, B.; Korzeniak, T.; Stefańczyk, O.; Pinkowicz, D.; Chorąży, S.; Podgajny, R.; Sieklucka, B. The impact of ligands upon topology and functionality of octacyanidometallate-based assemblies. *Coord. Chem. Rev.* **2012**, *256*, 1946–1971. [CrossRef]

5. Wang, X.-Y.; Avendaño, C.; Dunbar, K.R. Malecular magnetic materials based on 4d and 5d transition metals. *Chem. Soc. Rev.* **2011**, *40*, 3213–3238. [CrossRef] [PubMed]

6. Entley, W.R.; Girolami, G.S. High-temperature molecular magnets based on cyanovanadate building blocks: Spontaneous magnetization at 230 K. *Science* **1995**, *268*, 397–402. [CrossRef] [PubMed]

7. Imoto, K.; Takemura, M.; Tokoro, H.; Ohkoshi, S. A Cyano-Bridged Vanadium-Niobium Bimetal Assembly Exhibiting a High Curie Temperature of 210 K. *Eur. J. Inorg. Chem.* **2012**, 2649–2652. [CrossRef]

8. Mizuno, M.; Ohkoshi, S.; Hashimoto, K. Electrochemical Synthesis of High-T_c, Colored, Magnetic Thin Films Composed of Vanadium(II/III)-Chromium(II) Hexacyanochromate(III). *Adv. Mater.* **2000**, *12*, 1955–1958. [CrossRef]

9. Ohkoshi, S.; Mizuno, M.; Hung, G.J.; Hashimoto, K. Magnetooptical Effects of Room Temperature Molecular-Based Magnetic Films Composed of Vanadium Hexacyanochromates. *J. Phys. Chem. B* **2000**, *104*, 9365–9367. [CrossRef]

10. Ferlay, S.; Mallah, T.; Ouahés, R.; Veillet, P.; Verdaguer, M. A room-temperature organometallic magnet based on Prossian blue. *Nature* **1995**, *378*, 701–703. [CrossRef]

11. Holmes, S.M.; Girolami, G.S. Sol-Gel Synthesis of $KV^{II}[Cr^{III}(CN)_6]\cdot 2H_2O$: A Crystalline Molecule-Based Magnet with a Magnetic Ordering Temperature above 100 °C. *J. Am. Chem. Soc.* **1999**, *121*, 5593–5594. [CrossRef]

12. Hatlevik, Ø.; Buschmann, W.E.; Zhang, J.; Manson, J.L.; Miller, J.S. Enhancement of the Magnetic Ordering Temperature and Air Stability of a Mixed Valent Vanadium Hexacyanochromate(III) Magnet to 99 °C (372 K). *Adv. Mater.* **1999**, *11*, 914–918. [CrossRef]

13. Ohkoshi, S.-I.; Iyoda, T.; Fujishima, A.; Hashimoto, K. Magnetic properties of mixed ferro-ferrimagnets composed of Prussian blue analogs. *Phys. Rev. B* **1997**, *56*, 11642–11652. [CrossRef]

14. Pinkowicz, D.; Podgajny, R.; Pełka, R.; Nitek, W.; Bałanda, M.; Makarewicz, M.; Czapla, M.; Żukowski, J.; Kapusta, C.; Zając, D.; et al. Iron(II)-octacyanoniobate(IV) ferromagnet with TC 43 K. *Dalton Trans.* **2009**, 7771–7777. [CrossRef] [PubMed]

15. Handzlik, G.; Sieklucka, B.; Pinkowicz, D. Cross-linking of cyanide magnetic coordination polymers by rational insertion of formate, cyanide or azide. *Dalton Trans.* **2018**. [CrossRef] [PubMed]

16. Herrera, J.M.; Franz, P.; Podgajny, R.; Pilkington, M.; Biner, M.; Decurtins, S.; Stoeckli-Evans, H.; Neels, A.; Grade, R.; Dromzee, Y.; et al. Three-dimensional bimetallic octacyanidometalates $[M^{IV}\{(\mu\text{-}CN)_4Mn^{II}(H_2O)_2\}_2\cdot 4H_2O]_n$ (M=Nb, Mo, W): Synthesis, single-crystal X-ray diffraction and magnetism. *C. R. Chim.* **2008**, *11*, 1192. [CrossRef]

17. Alvarez, S.; Alemany, P.; Casanova, D.; Cirera, J.; Llunell, M.; Avnir, D. Shape maps and polyhedral interconversion paths in transition metal chemistry. *Coord. Chem. Rev.* **2005**, *249*, 1693–1708. [CrossRef]

18. Handzlik, G.; Magott, M.; Sieklucka, B.; Pinkowicz, D. Alternative Synthetic Route to Potassium Octacyanidoniobate(IV) and Its Molybdenum Congener. *Eur. J. Inorg. Chem.* **2016**, *30*, 4872–4877. [CrossRef]

19. Sheldrick, G.M. A short history of SHELX. *Acta Crystallogr. Sect. A: Found. Crystallogr.* **2008**, *64*, 112–122. [CrossRef] [PubMed]

20. Sheldrick, G.M. Crystal structure refinement with SHELXL. *Acta Crystallogr. Sect. C: Struct. Chem.* **2015**, *71*, 3–8. [CrossRef] [PubMed]

21. Llunell, M.; Casanova, D.; Cirera, J.; Alemany, P.; Alvarez, S. *SHAPE v. 2.1*; University of Barcelona: Barcelona, Spain, 2013.